Pattern selection for Darcy-Bénard convection with local thermal nonequilibrium

Biliana Bidin[(1,2)], **D. Andrew S. Rees**[2]

[(1)] *Institute of Engineering Mathematics, Universiti Malaysia Perlis, Kangar, Malaysia*
[(2)] *Department of Mechanical Engineering, University of Bath, Bath BA2 7AY, UK*

✉ Biliana@unimap.edu.my, D.A.S.Rees@bath.ac.uk

Abstract

A weakly nonlinear analysis is performed on the classical Darcy-Bénard problem to determine the effects of local thermal nonequilibrium on the planform of convection immediately post-onset. It is found that two-dimensional rolls are always favoured. Although disturbances which are perpendicular to the roll whose stability is being assessed usually form the most dangerous mode of instability, it is also found that there are regions of parameter space where the cross-roll instability becomes inoperative as an instability mechanism.

Keywords: Porous medium, convection, local thermal nonequilibrium, instability, weakly nonlinear, pattern selection.

Nomenclature

A, B	roll amplitudes
c	heat capacity
c_1 to c_4	Landau coefficients
c.c.	denoting complex conjugate
d	height of the layer
f, g, h	reduced P, Θ and Φ
$\mathcal{F}_1$, $\mathcal{G}_1$, $\mathcal{H}_1$	variables used for minimisation of Ra_0
g	gravity
h	dimensional heat transfer coefficient
H	nondimensional heat transfer coefficient
k	wavenumber of convection
k_f	thermal conductivity of fluid
k_s	thermal conductivity of solid
K	permeability
m_1 to m_{12}	constants in weakly nonlinear theory
p	pressure
P	perturbation pressure
$\mathcal{R}_1$, $\mathcal{R}_2$, $\mathcal{R}_3$	right hand sides in Eqs.(60)–(62)
Ra	Darcy-Rayleigh number (fluid phase)
Ra^*	Darcy-Rayleigh number (porous medium)
t	time
T	dimensional temperature
u, v	horizontal velocities
w	vertical velocity
x, y	horizontal coordinates
z	vertical coordinate

Greek symbols

α	diffusivity ratio
β	volumetric expansion coefficient
γ	porosity-modified conductivity ratio
$\delta A, \delta B$	disturbances in stability analysis
ϵ	small quantity
θ	nondimensional fluid temperature
Θ	perturbation fluid temperature
μ	dynamic viscosity
ρ	density
φ	porosity

ϕ	nondimensional solid temperature	cold	cold
Φ	perturbation solid temperature	f	fluid
χ	angle between the rolls	hot	hot
Ω	interaction coefficient	s	solid
		$\hat{}$	dimensional quantity
Subscripts, superscripts, and other symbols		$\overline{}$	complex conjugate
$0, 1, 2, 3, 4$	terms in the weakly nonlinear analysis	$'$	derivative with respect to z

1 Introduction

We shall consider how local thermal nonequilibrium (LTNE) effects affect the classical Darcy-Bénard problem, i.e. a uniform porous layer of constant thickness which is heated from below and cooled from above, and where the bounding temperatures are held constant in both time and space. Local thermal non-equilibrium is that special state whereby the use of a single heat transport equation is insufficient to model the microscopic heat transfer between the solid and fluid phases; in such cases two heat transport equations are used, one for each phase, and the system is closed by the addition of source/sink terms that are proportional to the temperature difference between the phases. This type of source/sink model was first introduced by Anzelius [1] and Schumann [2] in the 1920s and it continues to be used extensively to this day.

Three new parameters appear when local thermal nonequilibrium is being considered: H, which is a scaled interphase rate of heat transfer, γ, which is a porosity-weighted conductivity ratio and α, a thermal diffusivity ratio. Generally, local thermal equilibrium (LTE) corresponds to having sufficiently large values of either H or γ. It is often thought that a large conductivity contrast between the phases implies LTE, but the correctness of this assertiondepends on the magnitude of any externally imposed time scales; see [3]. Likewise, it is often assumed that LTE also arises when the flow is steady, but the works of Rees et al. [4] and Rees and Bassom [5] on the flushing of cold fluid using a hot fluid source, and the free convective boundary layer analyses of Rees and Pop [6] and Rees [7], show that LTNE effects persist for a wide range of values of both H and γ. Finally, we note that LTE is approached as the ratio between the microscopic and the macroscopic length scales tends to zero; the smaller microscales allow for a more rapid exchange of heat between the phases [8,9]. But these matters are well-known and are now quite well-developed; see Nield and Bejan [10], Rees and Pop [11] and Kuznetsov [12].

In the general field of stability theory it is usual for studies to begin with the description of the basic state, followed by a consideration of the onset of instability by means of a linearised analysis. Then various types of nonlinear analysis are used, such as weakly nonlinear theory, energy stability theory and fully numerical simulations. But for the title topic, namely the effect of local thermal nonequilibrium on Darcy-Bénard convection, the very first publications presented some strongly nonlinear computations without the benefit of knowing the context provided by a linearised theory; see Combarnous [13] and Combarnous and Bories [14]. It was some time later that Banu and Rees [15] embarked on a comprehensive study of the onset problem. Like the classical Darcy-Bénard problem, there is an analytical expression for the critical Darcy-Rayleigh number, but a simple Newton-Raphson scheme is then required to minimise its value over the wavenumber.

A rather large number of papers have followed the appearance of Banu and Rees [15] by solving the linear instability problem for different variations of the Darcy-Bénard problem with LTNE. For example,

Postelnicu and Rees [16], Postelnicu [17] and Malashetty et al. [18] considered how Brinkman effects alter the results of Banu and Rees [15]; generally, the addition of these effects serves to increase the critical Darcy-Rayleigh number because of the additional resistance to flow. Barletta and Rees [19] considered the effect of isoflux boundaries, and found that there is a region in (H, γ)-space where the critical wavenumber is zero, a result which is consistent with the LTE form of the stability problem discussed in §6.2 of Nield and Bejan [10]. However, in the remaining part of parameter space the critical wavenumber is nonzero. Nouri-Borujerdi et al. [20] studied the consequence of having internal heat generation within the layer, while a very recent work by Lagziri and Bezzazi [21] considers a case which effects a transition between cases studied by Banu and Rees [15] and Barletta and Rees [19] by employing thermal boundary conditions of the third kind. Celli et al. [22] have also considered the effect of an open upper surface. The work of Banu and Rees [15] has also been re-examined by Straughan [23] using an energy stability theory and this work confirms the absence of subcritical instabilities. Further papers may also be found which also include the effects of inclination, of anisotropy, rotation, unsteady heating and so on.

In the present paper our focus is solely on the use of a weakly nonlinear analysis of the cross-roll instability to determine whether rolls always form the preferred convective planform. The identity of the preferred pattern will inform the direction of further work on this topic.

2 Governing Equations

The main interest of this study is to investigate the onset and subsequent development of Darcy-Bénard convection in a horizontal porous layer when the solid and fluid phases are not in local thermal equilibrium. Thus we consider unsteady three-dimensional convection when the local thermal non-equilibrium (LTNE) two-field model is valid, and where the lower bounding surface is held at the constant temperature, $T_{\rm hot}$, while the upper surface is held at the lower temperature, $T_{\rm cold}$. The governing equations for Darcy-Bénard convection where a two-field model of microscopic heat transfer applies are given by Nield and Bejan [10]:

$$\frac{\partial \hat{u}}{\partial \hat{x}} + \frac{\partial \hat{v}}{\partial \hat{y}} + \frac{\partial \hat{w}}{\partial \hat{z}} = 0. \tag{1}$$

$$\hat{u} = -\frac{K}{\mu}\frac{\partial \hat{p}}{\partial \hat{x}}, \tag{2}$$

$$\hat{v} = -\frac{K}{\mu}\frac{\partial \hat{p}}{\partial \hat{y}}, \tag{3}$$

$$\hat{w} = -\frac{K}{\mu}\frac{\partial \hat{p}}{\partial \hat{z}} + \frac{\rho_f g \beta K}{\mu}(T_f - T_{\rm cold}), \tag{4}$$

$$\varphi(\rho c)_f \frac{\partial T_f}{\partial \hat{t}} + (\rho c)_f \Big(\hat{u}\frac{\partial T_f}{\partial \hat{x}} + \hat{v}\frac{\partial T_f}{\partial \hat{y}} + \hat{w}\frac{\partial T_f}{\partial \hat{z}} \Big) = \varphi k_f \Big(\frac{\partial^2 T_f}{\partial \hat{x}^2} + \frac{\partial^2 T_f}{\partial \hat{y}^2} + \frac{\partial^2 T_f}{\partial \hat{z}^2} \Big) + h(T_s - T_f), \tag{5}$$

$$(1-\varphi)(\rho c)_s \frac{\partial T_s}{\partial \hat{t}} = (1-\varphi) k_s \Big(\frac{\partial^2 T_s}{\partial \hat{x}^2} + \frac{\partial^2 T_s}{\partial \hat{y}^2} + \frac{\partial^2 T_s}{\partial \hat{z}^2} \Big) + h(T_f - T_s). \tag{6}$$

In the above $\hat{x}$ and $\hat{y}$ are horizontal coordinates while $\hat{z}$ is the vertical coordinate; the three respective velocities are $\hat{u}$, $\hat{v}$ and $\hat{w}$. In addition, $\hat{p}$ is the pressure, T the temperature and $\hat{t}$ is time. The subscripts, f and s, denote fluid and solid, respectively. Other properties of the fluid and solid phases are as follows: ρ is the density, β is the coefficient of cubical expansion, K is the permeability, μ is the dynamic viscosity, φ is the porosity, c is the specific heat, k is the thermal conductivity and g is the gravitational acceleration.

We assume that the phases have identical temperatures at the bounding surfaces and that the layer has depth, d. The boundary conditions are that,

$$\hat{w} = 0, \quad T_f = T_s = T_{\rm hot} \quad \text{on } \hat{z} = 0, \qquad\qquad \hat{w} = 0, \quad T_f = T_s = T_{\rm cold} \quad \text{on } \hat{z} = d. \tag{7}$$

The resulting three-dimensional flow given by solutions of Eqs. (1) to (6) may be studied by first introducing the following scalings,

$$(\hat{x}, \hat{y}, \hat{z}) = d(x, y, z), \qquad (\hat{u}, \hat{v}, \hat{w}) = \frac{\varphi k_f}{d(\rho c)_f}(u, v, w), \qquad \hat{p} = \frac{\mu k_f}{K(\rho c)_f} p, \tag{8}$$

$$\hat{t} = \frac{(\rho c)_f d^2}{k_f} t, \qquad (T_f, T_s) = T_{\rm cold} + (T_{\rm hot} - T_{\rm cold})(\theta, \phi). \tag{9}$$

After substitution of Eqs. (8) and (9) into Eqs. (1)-(6) and the elimination of the velocity terms we obtain the following non-dimensionalised pressure/temperature formulation of the governing equations,

$$\frac{\partial^2 p}{\partial x^2} + \frac{\partial^2 p}{\partial y^2} + \frac{\partial^2 p}{\partial z^2} = {\rm Ra}\, \frac{\partial \theta}{\partial z}, \tag{10}$$

$$\frac{\partial \theta}{\partial t} - \frac{\partial p}{\partial x}\frac{\partial \theta}{\partial x} - \frac{\partial p}{\partial y}\frac{\partial \theta}{\partial y} - \frac{\partial p}{\partial z}\frac{\partial \theta}{\partial z} + {\rm Ra}\, \theta \frac{\partial \theta}{\partial z} = \frac{\partial^2 \theta}{\partial x^2} + \frac{\partial^2 \theta}{\partial y^2} + \frac{\partial^2 \theta}{\partial z^2} + H(\phi - \theta), \tag{11}$$

$$\alpha \frac{\partial \phi}{\partial t} = \frac{\partial^2 \phi}{\partial x^2} + \frac{\partial^2 \phi}{\partial y^2} + \frac{\partial^2 \phi}{\partial z^2} + H\gamma(\theta - \phi). \tag{12}$$

Here θ and ϕ are the scaled temperatures of the fluid and solid phases, respectively, while the four governing nondimensional parameters are,

$$H = \frac{hd^2}{\varphi k_f}, \qquad \gamma = \frac{\varphi k_f}{(1-\varphi)k_s}, \qquad \alpha = \frac{k_f(\rho c)_s}{k_s(\rho c)_f} \qquad \text{and} \qquad {\rm Ra} = \frac{\rho_f g \beta K (T_{\rm hot} - T_{\rm cold}) d (\rho c)_f}{\varphi \mu k_f}. \tag{13}$$

In turn these quantities are the inter-phase heat transfer coefficient, the porosity-modified conductivity ratio, the diffusivity ratio and the Darcy-Rayleigh number. This last quantity is one which depends solely on the density, heat capacity and thermal conductivity of the fluid. When the two phases are in local thermal equilibrium, the usual porous-medium-based Darcy-Rayleigh number will be given by

$${\rm Ra}^* = \frac{{\rm Ra}\,\gamma}{1+\gamma} = \frac{\rho_{\rm pm} g \beta K (T_{\rm hot} - T_{\rm cold}) d (\rho c)_{\rm f}}{\mu k_{\rm pm}}. \tag{14}$$

Equations (10) to (12) are to be solved subject to the boundary conditions,

$$\frac{\partial p}{\partial z} = {\rm Ra}, \quad \theta = 1, \quad \phi = 1 \qquad \text{on } z = 0, \tag{15}$$

$$\frac{\partial p}{\partial z} = 0, \quad \theta = 0, \quad \phi = 0 \qquad \text{on } z = 1. \tag{16}$$

We note that the above boundary conditions for p may be obtained from the nondimensional form of Eq. (4) and using a zero vertical velocity.

3 Perturbation Equations

It is seen readily that the full system, Eqs. (10) to (12), is satisfied by the solution,

$$p = \mathrm{Ra}(z - \tfrac{1}{2}z^2), \qquad \theta = \phi = 1 - z. \tag{17}$$

We may now concentrate on the behaviour of convection cells by perturbing about this basic state: let

$$\begin{pmatrix} p \\ \theta \\ \phi \end{pmatrix} = \begin{pmatrix} \mathrm{Ra}(z - \frac{1}{2}z^2) \\ 1 - z \\ 1 - z \end{pmatrix} + \begin{pmatrix} P \\ \Theta \\ \Phi \end{pmatrix}, \tag{18}$$

where the disturbances, P, Θ and Φ, are asymptotically small in magnitude. Our analysis of the cross-roll instability begins by making the assumption that the Darcy-Rayleigh number is slightly larger than the critical value for the onset of convection. More specifically, we set,

$$\mathrm{Ra} = \mathrm{Ra}_0 + \epsilon^2 \mathrm{Ra}_2 + \cdots, \tag{19}$$

where $\epsilon \ll 1$ in magnitude and where Ra_0 is the critical Darcy-Rayleigh number. We also need to introduce a slow timescale according to,

$$\tau = \tfrac{1}{2}\epsilon^2 t, \tag{20}$$

where the numerical factor is an *a posteriori* adjustment so that the final Landau equation for a single roll has solely unit coefficients when LTE conditions prevail. The disturbance equations now take the form,

$$\frac{\partial^2 P}{\partial x^2} + \frac{\partial^2 P}{\partial y^2} + \frac{\partial^2 P}{\partial z^2} - \mathrm{Ra}_0 \frac{\partial \Theta}{\partial z} = \epsilon^2 \mathrm{Ra}_2 \frac{\partial \Theta}{\partial z}, \tag{21}$$

$$\frac{\partial^2 \Theta}{\partial x^2} + \frac{\partial^2 \Theta}{\partial y^2} + \frac{\partial^2 \Theta}{\partial z^2} + H(\Phi - \Theta) + \mathrm{Ra}_0\,\Theta - \frac{\partial P}{\partial z} = -\frac{\partial P}{\partial x}\frac{\partial \Theta}{\partial x} - \frac{\partial P}{\partial y}\frac{\partial \Theta}{\partial y} - \frac{\partial P}{\partial z}\frac{\partial \Theta}{\partial z} + (\mathrm{Ra}_0 + \epsilon^2 \mathrm{Ra}_2)\Theta \frac{\partial \Theta}{\partial z} + \tfrac{1}{2}\epsilon^2 \frac{\partial \Theta}{\partial \tau} \tag{22}$$

$$\frac{\partial^2 \Phi}{\partial x^2} + \frac{\partial^2 \Phi}{\partial y^2} + \frac{\partial^2 \Phi}{\partial z^2} + H\gamma(\Theta - \Phi) = \tfrac{1}{2}\epsilon^2 \alpha \frac{\partial \Phi}{\partial \tau}. \tag{23}$$

These equations, which have been arranged so that the left hand side consists of those terms which are required for linearised stability theory, are to be solved subject $P_z = \Theta = \Phi = 0$ on both $z = 0$ and $z = 1$.

Solutions to Eqs. (21) to (23) then take the form of a power series in ϵ:

$$\begin{pmatrix} P \\ \Theta \\ \Phi \end{pmatrix} = \epsilon \begin{pmatrix} P_1 \\ \Theta_1 \\ \Phi_1 \end{pmatrix} + \epsilon^2 \begin{pmatrix} P_2 \\ \Theta_2 \\ \Phi_2 \end{pmatrix} + \epsilon^3 \begin{pmatrix} P_3 \\ \Theta_3 \\ \Phi_3 \end{pmatrix} + \cdots. \tag{24}$$

4 Linear Stability Theory

The linear stability analysis corresponds to solving for the $O(\epsilon)$ terms in Eq. (24). It is this which forms the subject of the work of Banu and Rees [15] and the following will summarise and show how their work is modified when using the present pressure/temperature formulation.

The $O(\epsilon)$ terms may be shown to satisfy,

$$\frac{\partial^2 P_1}{\partial x^2} + \frac{\partial^2 P_1}{\partial y^2} + \frac{\partial^2 P_1}{\partial z^2} - \mathrm{Ra}_0 \frac{\partial \Theta_1}{\partial z} = 0, \tag{25}$$

$$\frac{\partial^2\Theta_1}{\partial x^2}+\frac{\partial^2\Theta_1}{\partial y^2}+\frac{\partial^2\Theta_1}{\partial z^2}+H(\Phi_1-\Theta_1)+\mathrm{Ra}_0\,\Theta_1-\frac{\partial P_1}{\partial z}=0, \tag{26}$$

$$\frac{\partial^2\Phi_1}{\partial x^2}+\frac{\partial^2\Phi_1}{\partial y^2}+\frac{\partial^2\Phi_1}{\partial z^2}+H\gamma(\Theta_1-\Phi_1)=0. \tag{27}$$

These equations may be found to have the following roll solutions,

$$\begin{pmatrix}P_1\\ \Theta_1\\ \Phi_1\end{pmatrix}=(Ae^{ikx}+\overline{A}e^{-ikx})\begin{pmatrix}m_1\cos\pi z\\ m_2\sin\pi z\\ m_3\sin\pi z\end{pmatrix}, \tag{28}$$

where k is the horizontal wavenumber of the rolls and where

$$m_1=-\frac{1}{\pi},\qquad m_2=\frac{k^2+\pi^2}{R_0\pi^2},\qquad m_3=\frac{H\gamma(k^2+\pi^2)}{(H\gamma+k^2+\pi^2)R_0\pi^2}. \tag{29}$$

The value chosen for m_1 is also such that, when a weakly nonlinear analysis is performed for the LTE case then the resulting Landau equation for the amplitude of convection is in canonical form, i.e. it has unit coefficients. The corresponding value of R_0 is given by

$$R_0=\frac{(k^2+\pi^2)^2}{k^2}\Big[\frac{H(1+\gamma)+k^2+\pi^2}{H\gamma+k^2+\pi^2}\Big]. \tag{30}$$

We note that the Local Thermal Equilibrium limit, $H\to\infty$, yields

$$R_0^*=\frac{\gamma}{1+\gamma}R_0=\frac{(k^2+\pi^2)^2}{k^2}. \tag{31}$$

This quantity represents the Darcy-Rayleigh based upon porous medium properties rather than on fluid properties. On the other hand, in the LTNE limit, $H\to 0$, where the thermal fields of the two phases no longer interact, we have

$$R_0=\frac{(k^2+\pi^2)^2}{k^2}. \tag{32}$$

In both cases the neutral curve is unimodal with a single minimum when $k=\pi$, and therefore the minimum values of the Darcy-Rayleigh numbers are,

$$R_0=4\pi^2,\qquad R_0^*=\frac{\gamma}{\gamma+1}4\pi^2. \tag{33}$$

Moreover Banu and Rees [15] noted that the neutral curves are unimodal in the whole (H,γ) parameter space and that the minimum needs to be computed using a simple Newton-Raphson scheme. For the sake of context Figs. 1 and 2 contain recomputed critical values and these show how the porous-medium-based Darcy-Rayleigh number and the wavenumber depend on H and γ.

Figure 1 shows how the minimised values of Ra_0^* vary with $\log_{10}H$ for different values of γ. The corresponding values of Ra_0 become extremely large ($\mathrm{Ra}_0\sim 4\pi^2(\gamma+1)/\gamma$) when γ takes small values, and therefore we selected to present the variation of Ra_0^*. Immediately we see that the LTE onset criterion is reproduced well when $\gamma\gg 10^2$ independently of the value of H. On the other hand, when γ takes very small values, LTE conditions are only achieved when H is substantially larger than γ^{-1}. that limit is in accord with with Eq. (31), namely that $\mathrm{Ra}_0=4\pi^2(\gamma+1)/\gamma$.

Figure 2 displays the corresponding critical wavenumbers, k_c. Apart from when γ takes values in excess of 10^{-1}, the variation of k_c takes an unusually large maximum value as H is varied. While the critical value is π in the LTE limit, it is approximately 12 when $\gamma=10^{-3}$, and it takes ever larger values as γ decreases further. The locus of these maxima is shown as a dotted line in Fig. 3. The asymptotic behaviour of this locus may be found in Banu and Rees [15].

5 Weakly Nonlinear Analysis

The aim now is to determine whether or not the convective roll which has been described in §4 forms the stable planform of convection. We shall not present a study of the Eckhaus or sideband instability of rolls — such an analysis is essentially identical in form to that presented in Newell and Whitehead [24] for the Rayleigh-Bénard problem. In such an analysis the band of stable wavenumbers for slightly postcritical roll convection is centred on the critical wavenumber and is of $\frac{1}{3}^{\text{rd}}$ of the width of the range of existence of rolls, as given by the neutral curve. Likewise, the zigzag instability is operative whenever the wavenumber of the rolls is less than the critical value. Rather, our aim is to consider the cross-roll instability mechanisn in order to determine whether rolls are stable or if some other pattern of convection exists.

To this end we shall consider the interaction of a pair of rolls with different orientations but which are otherwise identical in form. Therefore we shall replace the single-roll solution of Eqs. (25) to (27) which is given in Eq. (28) by the following,

$$\begin{pmatrix} p_1 \\ \Theta_1 \\ \Phi_1 \end{pmatrix} = \begin{pmatrix} f_1(z) \\ g_1(z) \\ h_1(z) \end{pmatrix} \Big[Ae^{ikx} + \text{c.c.} + Be^{ik(x\cos\chi - y\sin\chi)} + \text{c.c.} \Big], \tag{34}$$

where χ is the angle between the axes of the rolls, and where the amplitudes, A and B, are functions solely of τ, the slow timescale which is defined in Eq. (20). In addition, the functions, $f_1(z)$, $g_1(z)$ and $h_1(z)$, are given precisely by the respective terms in the right hand side vector in Eq. (28).

The solutions given in Eq. (34) now form the $O(\epsilon)$ terms in the expansion given in Eq. (24). Given that the full system of equations that we are studying is nonlinear, further terms in that expansion consist of self-interactions and mutual interactions. We have relegated the details of this analysis to the Appendix where we have provided both the reduced systems of ODEs for each interaction term and their analytical solutions. As a check for the rather detailed analytical solutions we also solved the ODEs (i.e. systems (45), (50), (51), (52) and (53), which may be found in the Appendix) using a shooting method in conjunction with the classical 4th order Runge-Kutta scheme. In addition system (46) was also solved simultaneously in order to find the minimum in the neutral curve. The analytical solutions and their numerical counterparts matched perfectly.

At $O(\epsilon^3)$ there arises the usual requirement for the application of a solvability condition; this was undertaken both analytically (using integrals) and numerically (by solving the appropriate set of ODEs). Again, the results obtained using these different methods coincide. The final amplitude equations for A and B which have been derived in the Appendix are reproduced here for convenience:

$$c_1 A_\tau = c_2 R_2 A - c_3 A^2 \overline{A} - c_4 A B \overline{B}, \tag{35}$$

$$c_1 B_\tau = c_2 R_2 B - c_3 B^2 \overline{B} - c_4 B A \overline{A}. \tag{36}$$

Detailed expressions for the constants, c_1 to c_4, which are always positive, may also be found in the Appendix. We define the coupling (or interaction) parameter, Ω, according to

$$\Omega(\chi; H, \gamma) = \frac{c_4}{c_3}. \tag{37}$$

For Darcy-Bénard convection this expression reduces to,

$$\Omega = \frac{70 + 28\cos^2\chi - 2\cos^4\chi}{49 - 2\cos^2\chi + \cos^4\chi}, \tag{38}$$

Given that all the constants, c_1 to c_4 are positive, then the bifurcation to convection as R_2 becomes positive is supercritical. This confirms the conclusions of the energy stability analysis of Straughan [23]. However is well-known that the some important stability properties of convecting systems depend greatly on the value of Ω and its variation with χ. For example, the papers by Riahi [25], Rees and Riley [26] and Rees and Mojtabi [27] all find regions of their respective parameter spaces within which convection in the form of two-dimensional rolls is unstable and that the preferred planform is square cells which consist of two systems of rolls at right angles to one another. The role played by the value of Ω may be illustrated briefly by considering the two solutions,

$$\text{rolls:} \qquad A = \sqrt{c_2 R_2/c_3}, \quad B = 0, \tag{39}$$

$$\text{rectangular cells:} \qquad A = B = \sqrt{c_2 R_2/(c_3 + c_4)}. \tag{40}$$

We may analyse the stability of roll solutions by perturbing the solution given in Eq. (39): let

$$A = \sqrt{c_2 R_2/c_3} + \delta A, \quad B = \delta B, \tag{41}$$

and where, for the sake of simplicity, we assume that the small perturbations, δA and δB, are both real. At leading order the equations for the evolution of these disturbances decouple and are,

$$c_1 \delta A_\tau = -2c_2 R_2\, \delta A, \qquad c_1 \delta B_\tau = \left(1 - \frac{c_4}{c_3}\right) R_2 \delta B. \tag{42}$$

The equation for δA shows that it will always decay exponentially with time. The equation for δB has the same conclusion unless $c_4 < c_3$, i.e. $\Omega < 1$, in which case these disturbances will grow. In such cases the ultimate steady state will be the pattern given in Eq. (40). If we relax the assumption that the disturbances are real, then we find that the A-roll is neutrally stable with respect to disturbances in phase, while the conclusion for the B-roll is unchanged. Should the minimum value of Ω be less than unity, then a similar analysis shows that square or rectangular cells form the stable planform and that rolls are unstable.

Given that Ω varies with the angle between the roll axes, then the most positive value for the growth rate, $\Omega - 1$, happens at that relative orientation which minimises Ω. This minimisation tends to occur when the rolls are orthogonal and it does so for the classical Darcy-Bénard problem: see Eq. (38) where Ω decreases from 2 when $\chi = 0$ down to $\Omega = {}^{10}\!/\!_{7}$ when $\chi = 90°$. This also happens for the Rayleigh-Bénard convection of an infinite Prandtl number fluid with stress-free surfaces (Newell and Whitehead [24]) where the corresponding form for Ω is

$$\Omega = 1 + \frac{(5 + \cos\chi)^2(1 - \cos\chi)^2}{(5 + \cos\chi)^3 - \frac{27}{4}(1 + \cos\chi)} + \frac{(5 - \cos\chi)^2(1 + \cos\chi)^2}{(5 - \cos\chi)^3 - \frac{27}{4}(1 - \cos\chi)}, \tag{43}$$

and therefore this Ω deceases from 2 when $\chi = 0$ down to $\frac{673}{473}$ when $\chi = 90°$. Clearly single rolls form the stable planform for these two convecting systems since $\min_\chi \Omega > 1$. In the above-mentioned papers, [25]-[27], $\min_\chi \Omega < 1$ and therefore three-dimensional convection ensues. Given the central role played by Ω in deciding the stable planform we shall now consider how it varies for the present case.

5.1 Variation of the interaction coefficient, Ω

Figure 3 shows how Ω varies with χ for a range of values of γ when $H = 10$. The lowest curve in that figure corresponds to the Local Thermal Equilibrium limit and it is also given by Eq. (38). The curves

rise very slightly as γ decreases towards zero but they retain the property that $\Omega = 2$ when $\chi = 0$, and that they decrease towards a value which is above unity as χ increases towards 90°. Thus rolls remain the stable planform when $H = 10$. We also note that the corresponding curves for smaller values of H display a smaller variation with γ.

Figures 4, 5 and 6 show the corresponding behaviour of Ω for $H = 100$, 1000 and 10000, respectively. For $H = 100$ we see immediately that Ω no longer varies monotonically when $\log_{10}\gamma$ is less than roughly -1. In such cases Ω begins to rise from 2 at first before eventually descending again to a value below 2, but which is above unity. Despite this novel form of variation of Ω, the cross-roll instability remains significant because $\min_\chi \Omega$ is below 2.

When $H = 1000$ (Figure 5) it becomes very evident that the manner in which the Ω-variation takes place is as follows: (i) when γ is sufficiently large Ω decreases monotonically with χ; (ii) as γ decreases the curvature at $\chi = 0°$ becomes positive so that Ω takes its maximum value within the range $0 < \chi < 90°$ but the minimum value at $\chi = 90°$ still lies in the range 1 to 2; (iii) as γ decreases still further the value of Ω at $\chi = 90°$ rises above 2 at which point $\chi = 0$ becomes the minimising value of χ. Therefore we have a discontinuous change from 90° to 0 in the value of χ which corresponds to the smallest value of Ω. Although it is not clear from a visual inspection of Fig. 6 this remains true for $H = 10000$. In this latter case we find that when $\log_{10}\gamma = -2.66648$ then $\Omega(\chi = 90°) = 2.0000$; given that the maximum value of Ω is approximately 2.037 we see that the variation in Ω is quite small for that choice of values of H and γ.

It is clear, therefore, that the (H, γ) parameter space is divided into two main regions, one where $\Omega_{\min} < 2$ with $\chi = 90°$ and the other where $\Omega_{\min} = 2$ with $\chi = 0$. The transition between having $\chi = 90°$ and having $\chi = 0$ as the minimising orientation is sudden. The border between the regions may be found by extending the previously-mentioned Newton-Raphson scheme by adding the extra equation $\Omega(\chi = 90°) - 2 = 0$ and by having either H or γ as the extra value to be found. The result of this straightforward process is shown in Fig. 7. The shaded region is where $\Omega_{\min} > 2$, and therefore the cross-roll instability is inoperative in this region. Thus, for any pair of values of H and γ, the variation of Ω with χ is monotonically increasing as χ increases from zero to 90°. The unshaded region then corresponds to where $\Omega_{\min} < 2$, and therefore the cross-roll instability may happen should the primary roll have its wavenumber detuned slightly from its critical value.

The dotted line in Fig. 7 corresponds to precisely where $d^2\Omega/d\chi^2 = 0$ at $\chi = 0$, i.e. the transition between where Ω decreases and where it increases as χ increases from zero. Therefore the region between the dotted line and the shaded region shows where the χ-dependence of Ω is not monotonic but has an S-shape similar to the uppermost curve in Fig. 4. Elsewhere Ω decreases monotonically such as is shown in Fig. 3.

Finally, Fig. 8 shows the variation of $\Omega(90°)$ with H for selected values of γ. It is clear that $\Omega > 1$ in all cases, and therefore the postcritical planform of convection takes the form of rolls in an unbounded domain, rather than a square ($\chi = 90°$) or rectangular ($0 < \chi < 90°$) pattern. Given our detailed analysis above, we emphasise again that when $\Omega > 2$ then the cross-roll instability is inoperative although the usual Eckhaus and zigzag instabilities described in Newell and Whitehead [24] may still arise depending on how much the wavenumber of the roll differs from its critical value.

6 Conclusions

We have undertaken a weakly nonlinear analysis of the onset of convection in the classical Darcy-Bénard problem where local thermal non-equilibrium effects are significant. Whilst the Eckhaus and zigzag instabilities may also be considered, the symmetries of the configuration are such that the conclusions of Newell and Whitehead [24] for the Rayleigh-Bénard problem also apply here and therefore we have not covered this aspect. Rather, we have considered the cross-roll instability mechanism in some detail using the standard approach of having two rolls with axes at different horizontal orientations.

This weakly nonlinear analysis of the cross-roll instability shows conclusively that rolls remain the stable planform for convection in the immediately postcritical regime for the whole of the (H, γ) parameter space, and that the onset of convection is supercritical. A rather unusual feature is that there is a region within this parameter space where the cross-roll instability ceases to arise; see Fig. 7.

The next step in the study of the effects of local thermal nonequilibrium on the Darcy-Bénard problem will be an assessment of strongly nonlinear convection, i.e. to undertake a systematic extension to the works of Combarnous [13] and Combarnous and Bories [14]. This will enable the determination of how local thermal nonequilibrium affects not only the postcritical heat transport, but also the eventual appearance of unsteady flows.

Appendix

The leading order disturbances, $(O(\epsilon))$ are taken to be of the form,

$$\begin{pmatrix} p_1 \\ \Theta_1 \\ \Phi_1 \end{pmatrix} = \begin{pmatrix} f_1(z) \\ g_1(z) \\ h_1(z) \end{pmatrix} \left[A e^{ikx} + \text{c.c.} + B e^{ik(x\cos\chi - y\sin\chi)} + \text{c.c.} \right] \tag{44}$$

which represents rolls with axes that are at an angle χ to one another. The z-dependent functions satisfy the equations,

$$\begin{aligned} &f_1'' - k^2 f_1 - \mathrm{Ra}_0\, g_1' = 0, \\ &g_1'' + (\mathrm{Ra}_0 - k^2) g_1 - f_1' + H(h_1 - g_1) = 0, \\ &h_1'' + H\gamma(g_1 - h_1) = 0, \end{aligned} \tag{45}$$

and they form an eigenvalue problem for Ra_0 as a function of the wavenumber, k. Solutions for f_1, g_1 and h_1 may be found in Eqs. (28) and (29), and value of Ra_0 as a function of k in Eq. (30).

Banu and Rees [15] solved the streamfunction/temperature version of these equations and found that the neutral curve is always unimodal and has a unique minimum. This minimum may be found numerically by solving them together with the system formed by taking the k-derivative of Eq. (45) and setting $d\mathrm{Ra}_0/dk = 0$. If we define $(\mathcal{F}_1, \mathcal{G}_1, \mathcal{H}_1) = d(f_1, g_1, h_1)/dk$, then we obtain,

$$\begin{aligned} &\mathcal{F}_1'' - k^2 \mathcal{F}_1 - \mathrm{Ra}_0\, \mathcal{G}_1' = 2k f_1, \\ &\mathcal{G}_1'' + (\mathrm{Ra}_0 - k^2)\mathcal{G}_1 - \mathcal{F}_1' + H(\mathcal{H}_1 - \mathcal{G}_1) = 2k g_1, \\ &\mathcal{H}_1'' + H\gamma(\mathcal{G}_1 - \mathcal{H}_1) = 0. \end{aligned} \tag{46}$$

Therefore the minimum in the neutral curve may be found by solving the systems (45) and (46) simultaneously subject to the boundary conditions,

$$f_1' = g_1 = h_1 = \mathcal{F}_1' = \mathcal{G}_1 = \mathcal{H}_1 = 0 \quad \text{on both } z = 0 \text{ and } z = 1, \tag{47}$$

and with the normalisation conditions,

$$f_1(0) = -\frac{1}{\pi} \quad \text{and} \quad \mathcal{F}_1(0) = \text{any constant}. \tag{48}$$

The normalisation for f_1 forces a nonzero solution which enables the computation of Ra_0, and is identical to that given for m_1 in Eq. (29). The computed value for k is independent of the constant used for $\mathcal{F}_1(0)$ although one generally uses zero for this. In the main text of this paper, this minimum was also obtained using a suitable Newton-Raphson scheme to minimise the critical Darcy-Rayleigh number given in Eq. (30). These alternative methods yield exactly the same results and agree perfectly with Banu and Rees [15].

At $O(\epsilon^2)$ the substitution is,

$$\begin{aligned}\begin{pmatrix} p_2 \\ \Theta_2 \\ \Phi_2 \end{pmatrix} &= \begin{pmatrix} f_0(z) \\ g_0(z) \\ h_0(z) \end{pmatrix} \Big[A\overline{A} + B\overline{B}\Big] + \begin{pmatrix} f_2(z) \\ g_2(z) \\ h_2(z) \end{pmatrix} \Big[A^2 e^{2ikx} + \text{c.c.} + B^2 e^{2ik(x\cos\chi - y\sin\chi)} + \text{c.c.}\Big] \\ &+ \begin{pmatrix} f_3(z) \\ g_3(z) \\ h_3(z) \end{pmatrix} \Big[A\overline{B} e^{ik(x(1-\cos\chi)+y\sin\chi)} + \text{c.c.}\Big] + \begin{pmatrix} f_4(z) \\ g_4(z) \\ h_4(z) \end{pmatrix} \Big[AB e^{ik(x(1+\cos\chi)-y\sin\chi)} + \text{c.c.}\Big].\end{aligned} \tag{49}$$

The f_j and g_j functions satisfy the equations,

$$\begin{aligned} &f_0'' - \mathrm{Ra}_0\, g_0' = 0, \\ &g_0'' + \mathrm{Ra}_0\, g_0 - f_0' + H(h_0 - g_0) = 2\Big[\mathrm{Ra}_0\, g_1 g_1' - f_1' g_1' - k^2 f_1 g_1\Big], \\ &h_0'' + H\gamma(g_0 - h_0) = 0, \end{aligned} \tag{50}$$

$$\begin{aligned} &f_2'' - 4k^2 f_2 - \mathrm{Ra}_0\, g_2' = 0, \\ &g_2'' + (\mathrm{Ra}_0 - 4k^2) g_2 - f_2' + H(h_2 - g_2) = \mathrm{Ra}_0\, g_1 g_1' - f_1' g_1' + k^2 f_1 g_1, \\ &h_2'' + H\gamma(g_2 - h_2) = 0, \end{aligned} \tag{51}$$

$$\begin{aligned} &f_3'' - k^2(2 - 2\cos\chi) f_3 - \mathrm{Ra}_0\, g_3' = 0, \\ &g_3'' + \Big[\mathrm{Ra}_0 - k^2(2 - 2\cos\chi)\Big] g_3 - f_3' + H(h_3 - g_3) = 2\Big[\mathrm{Ra}_0\, g_1 g_1' - f_1' g_1' - k^2 f_1 g_1 \cos\chi\Big], \\ &h_3'' + H\gamma(g_3 - h_3) = 0, \end{aligned} \tag{52}$$

$$\begin{aligned} &f_4'' - k^2(2 + 2\cos\chi) f_4 - \mathrm{Ra}_0\, g_4' = 0, \\ &g_4'' + \Big[\mathrm{Ra}_0 - k^2(2 + 2\cos\chi)\Big] g_4 - f_4' + H(h_4 - g_4) = 2\Big[\mathrm{Ra}_0\, g_1 g_1' - f_1' g_1' + k^2 f_1 g_1 \cos\chi\Big], \\ &h_4'' + H\gamma(g_4 - h_4) = 0, \end{aligned} \tag{53}$$

while the boundary conditions are,

$$f_j' = g_j = h_j = 0 \quad \text{on } z = 0 \text{ and } z = 1 \text{ for } j = 0, 2, 3, 4. \tag{54}$$

The respective solutions are,

$$\begin{pmatrix} f_0 \\ g_0 \\ h_0 \end{pmatrix} = \begin{pmatrix} m_4 \cos 2\pi z \\ m_5 \sin 2\pi z \\ m_6 \sin 2\pi z \end{pmatrix}, \qquad \begin{pmatrix} f_2 \\ g_2 \\ h_2 \end{pmatrix} = \begin{pmatrix} 0 \\ 0 \\ 0 \end{pmatrix}, \qquad \begin{pmatrix} f_3 \\ g_3 \\ h_3 \end{pmatrix} = \begin{pmatrix} m_7 \cos 2\pi z \\ m_8 \sin 2\pi z \\ m_9 \sin 2\pi z \end{pmatrix}, \qquad \begin{pmatrix} f_4 \\ g_4 \\ h_4 \end{pmatrix} = \begin{pmatrix} m_{10} \cos 2\pi z \\ m_{11} \sin 2\pi z \\ m_{12} \sin 2\pi z \end{pmatrix}, \tag{55}$$

where the constants, m_4 to m_{12} are given by,

$$\begin{pmatrix} m_4 \\ m_5 \\ m_6 \end{pmatrix} = \frac{2k^2 m_2}{4\pi^3} \frac{1}{H(\gamma+1)+4\pi^2} \begin{pmatrix} (R_0/2\pi)(H\gamma+4\pi^2) \\ -H\gamma \\ -(H\gamma+4\pi^2) \end{pmatrix} \tag{56}$$

$$\begin{pmatrix} m_7 \\ m_8 \\ m_9 \end{pmatrix} = \frac{k^2 m_2 (1+\cos\chi)/\pi}{R_0(\xi+H\gamma)+2k^2(1-\cos\chi)-\xi^2(\xi+H(\gamma+1))} \begin{pmatrix} -2\pi R_0(\xi+H\gamma) \\ \xi(\xi+H\gamma) \\ \xi H\gamma \end{pmatrix}, \qquad (\xi = 4\pi^2+2k^2(1-\cos\chi)), \tag{57}$$

$$\begin{pmatrix} m_{10} \\ m_{11} \\ m_{12} \end{pmatrix} = \frac{k^2 m_2 (1-\cos\chi)/\pi}{R_0(\xi+H\gamma)+2k^2(1+\cos\chi)-\xi^2(\xi+H(\gamma+1))} \begin{pmatrix} -2\pi R_0(\xi+H\gamma) \\ \xi(\xi+H\gamma) \\ \xi H\gamma \end{pmatrix}, \qquad (\xi = 4\pi^2+2k^2(1+\cos\chi)). \tag{58}$$

Once more, these expressions were validated by comparison with the numerical solutions of Eqs. (50) to (53).

At third order in the expansion of Eqs. (21) to (23) we obtain the following system,

$$\begin{aligned} \nabla^2 P_3 - R_0\,\Theta_{3,z} &= R_2\Theta_1, \\ \nabla^2\Theta_3 + R_0\Theta_3 - P_{3,z} + H(\Phi_3-\Theta_3) &= R_0(\Theta_1\Theta_{2,z}+\Theta_2\Theta_{1,z}) + \tfrac{1}{2}\Theta_{1,\tau} - R_2\Theta_1 - \nabla P_1.\nabla\Theta_2 - \nabla P_2.\nabla\Theta_1, \\ \nabla^2\Phi_3 + H\gamma(\Theta_3-\Phi_3) &= \tfrac{1}{2}\alpha\Phi_{1,\tau}. \end{aligned} \tag{59}$$

The number of inhomogeneous terms becomes quite large and therefore they will be omitted here. Of more interest are those terms which are proportional to the eigensolutions of the $O(\epsilon)$ equations. Indeed, we need only to concentrate on those which are in the same orientation as roll-A, given the symmetry between the rolls. If we write the $O(\epsilon^3)$ equations in the form,

$$\frac{\partial^2 P_3}{\partial x^2} + \frac{\partial^2 P_3}{\partial y^2} + \frac{\partial^2 P_3}{\partial z^2} - \mathrm{Ra}_0 \frac{\partial \Theta_3}{\partial z} = \mathcal{R}_1 e^{ikx} + \text{c.c.}, \tag{60}$$

$$\frac{\partial^2 \Theta_3}{\partial x^2} + \frac{\partial^2 \Theta_3}{\partial y^2} + \frac{\partial^2 \Theta_3}{\partial z^2} + H(\Phi_3-\Theta_3) + \mathrm{Ra}_0\,\Theta_3 - \frac{\partial P_3}{\partial z} = \mathcal{R}_2 e^{ikx} + \text{c.c}, \tag{61}$$

$$\frac{\partial^2 \Phi_3}{\partial x^2} + \frac{\partial^2 \Phi_3}{\partial y^2} + \frac{\partial^2 \Phi_3}{\partial z^2} + H\gamma(\Theta_3-\Phi_3) = \mathcal{R}_3 e^{ikx} + \text{c.c}, \tag{62}$$

then multiply both sides of each equation by the respective terms in Eq. (28) which involve e^{-ikx}, integrate between $z=0$ and $z=1$, and add the equations with the appropriate weightings, then we obtain the solvability condition,

$$\int_0^1 \Big[-\frac{m_1 \mathcal{R}_1 \cos\pi z}{R_0} + m_2 \mathcal{R}_2 \sin\pi z + \frac{m_3 \mathcal{R}_3 \sin\pi z}{\gamma} \Big]\, dz = 0. \tag{63}$$

The result of this lengthy process is the following Landau equation,

$$c_1 A_\tau = c_2 R_2 A - c_3 A^2 \overline{A} - c_4 A B \overline{B}, \tag{64}$$

and, by symmetry, the Landau equation for the B-roll is,

$$c_1 B_\tau = c_2 R_2 B - c_3 B^2 \overline{B} - c_4 B A \overline{A}, \tag{65}$$

where the constants, c_1 to c_4, are given by

$$c_1 = \frac{m_2}{2} + \alpha \left[\frac{m_3}{2 m_2 \gamma} \right], \qquad c_2 = m_2 + \frac{\pi m_1}{R_0}, \tag{66}$$

$$c_3 = m_2 m_4 \pi^2 - m_5 (m_1 \pi^2 + \tfrac{1}{2} m_2 R_0 \pi) \tag{67}$$

and

$$\begin{aligned} c_4 = {} & \tfrac{1}{2} k^2 (1 + \cos\chi)(m_2 m_{10} - m_1 m_{11}) + (m_4 + m_7 + m_{10}) m_2 \pi^2 \\ & + \tfrac{1}{2} k^2 (1 - \cos\chi)(m_2 m_7 - m_1 m_8) - (m_5 + m_8 + m_{11})(m_1 \pi^2 + \tfrac{1}{2} m_2 \pi R_0). \end{aligned} \tag{68}$$

We note that all of these coefficients are positive and therefore the onset of convection is supercritical. Of most interest is the ratio,

$$\Omega(\chi; H, \gamma) = c_4 / c_3, \tag{69}$$

which determines whether single roll solutions (such as $A = \sqrt{R_2 c_2 / c_3}$, $B = 0$) form the stable planform of convection, or whether square cells (such as $A = B = \sqrt{R_2 c_2 / (c_3 + c_4)}$ with $\chi = 90°$) do.

Finally, we note that it is also possible to obtain the solvability condition by writing out the ordinary differential equations in full and solving them numerically where the constants c_1 to c_4 are computed by regarding them as being eigenvalues; once more these computations served to validate the analytical expressions.

References

[1] Anzelius, A.: Über Erwärmung vermittels durchströmender Medien. *Zeit. Math. Mech.*, **6**, 291-294 (1926).

[2] Schumann, T.E.W.: Heat transfer: a liquid flowing through a porous prism. *J. Franklin Institute*, **208**, 405-416 (1929).

[3] Minkowycz, W.J., Haji-Sheikh, A., Vafai, K.: On the departure from local thermal equilibrium in porous media due to a rapidly changing heat source: the Sparrow number. *International Journal of Heat and Mass Transfer*, **42(18)**, 3373-3385 (1999).

[4] Rees, D.A.S., Bassom, A.P., Siddheshwar, P.G.: Local thermal non-equilibrium effects arising from the injection of a hot fluid into a porous medium. *Journal of Fluid Mechanics*, **594**, 379-398 (2008).

[5] Rees, D.A.S., Bassom, A.P.: The radial injection of a hot fluid into a cold porous medium: the effects of local thermal non-equilibrium. *Computational Thermal Sciences*, **2(3)**, 221-230 (2010).

[6] Rees, D.A.S., Pop, I.: Vertical free convective boundary-layer flow in a porous medium using a thermal nonequilibrium model. *Journal of Porous Media*, **3**, 31-44 (2000).

[7] Rees, D.A.S.: Vertical free convective boundary-layer flow in a porous medium using a thermal nonequilibrium model: elliptical effects. *J. Appl. Math. Phys. (ZAMP)*, **54**, 437-448 (2003).

[8] Rees, D.A.S.: Microscopic modelling of the two-temperature model for conduction in heterogeneous media. *Journal of Porous Media*, **13**, 125-143 (2010).

[9] Rees, D.A.S.: "Microscopic modelling of the two-temperature model for conduction in heterogeneous media: three-dimensional media" in Proceedings of the 4th International Conference on Applications of Porous Media, Istanbul, Turkey, Paper 15 (2009).

[10] Nield, D.A., Bejan, A.: Convection in Porous Media (5th Edition). Springer, (2017).

[11] Rees, D.A.S., Pop, I.: "Local thermal nonequilibrium in porous medium convection." In: Transport Phenomena in Porous Media III (eds. D.B.Ingham and I.Pop) pp.147-173. Pergamon, (2005).

[12] Kuznetsov, A.V.: "Thermal nonequilibrium forced convection in porous media." In: Transport Phenomena in Porous Media I (eds. D.B.Ingham and I.Pop) pp.103-129. Pergamon, (1998).

[13] Combarnous, M.: Description du transfert de chaleur par convection naturelle dans une couche poreuse horizontale á l'aide d'un coefficient de transfert fluide-solide. *C. R. Acad. Sci. Paris II Ser. A*, **275**, 1375-1378 (1972).

[14] Combarnous, M., Bories, S.: Modelisation de la convection naturelle au sein d'une couche poreuse horizontale a l'aide d'un coefficient de transfert solide-fluide. *International Journal of Heat and Mass Transfer*, **17(4)**, 505-515 (1974).

[15] Banu, N., Rees, D.A.S.: The onset of Darcy-Bénard convection using a thermal nonequilibrium model. *International Journal of Heat Mass Transfer*, **45**, 2221-2228 (2002).

[16] Postelnicu, A., Rees, D.A.S.: The onset of Darcy-Brinkman convection in a porous layer using a thermal nonequlibrium model - Part I: Stress-free boundaries. *International Journal of Energy Research*, **27(10)**, 961-973 (2003).

[17] Postelnicu, A.: The onset of a Darcy-Brinkman convection using a thermal nonequilibrium model. Part II. *International Journal of Thermal Sciences*, **47(12)**, 1587-1594 (2008).

[18] Malashetty, M.S., Shivakumara, I.S., Kulkarni, S.: The onset of Lapwood.Brinkman convection using a thermal non-equilibrium model. *International Journal of Heat and Mass Transfer*, **48**, 1155-1163 (2005).

[19] Barletta, A., Rees, D.A.S.: Local thermal non-equilibrium effects in the Darcy-Bénard instability with isoflux boundary conditions. *International Journal of Heat and Mass Transfer*, **55**, 384-394 (2012).

[20] Nouri-Borujerdi, A., Noghrehabadi, A.R., Rees, D.A.S.: The onset of convection in a horizontal porous layer with uniform heat generation using a thermal non-equilibrium model. *Transport in Porous Media*, **69**, 343-357 (2007).

[21] Lagziri, H., Bezzazi, M.: Robin boundary effect in the Darcy-Rayleigh problem with local thermal equilibrium model. *Transport in Porous Media*, **129**, 701-720 (2019).

[22] Celli, M., Lagziri, H., Bezzazi, M.: Local thermal non-equilibrium effects in the Horton-Rogers-Lapwood problem with a free surface. *International Journal of Thermal Sciences*, **116**, 254-264 (2017).

[23] Straughan, B.: Global nonlinear stability in porous convection with a thermal non-equilibrium model. *Proceedings of The Royal Society A*, **462**, 409-418 (2005).

[24] Newell, A.C., Whitehead, J.A.: Finite bandwidth, finite amplitude convection. *Journal of Fluid Mechanics*, **38**, 279-303 (1969).

[25] Riahi, N.: Nonlinear convection in a porous layer with finite conducting boundaries. *Journal of Fluid Mechanices*, **129**, 153-171 (1983).

[26] Rees, D.A.S., Riley, D.S.: The three-dimensional stability of finite-amplitude convection in a layered porous medium heated from below. *Journal of Fluid Mechanics*, **211**, 437–461 (1990).

[27] Rees, D.A.S., Mojtabi, A.: The effect of conducting boundaries on weakly nonlinear Darcy-Bénard convection. *Transport in Porous Media*, **88**, 45-63 (2011).

Figures

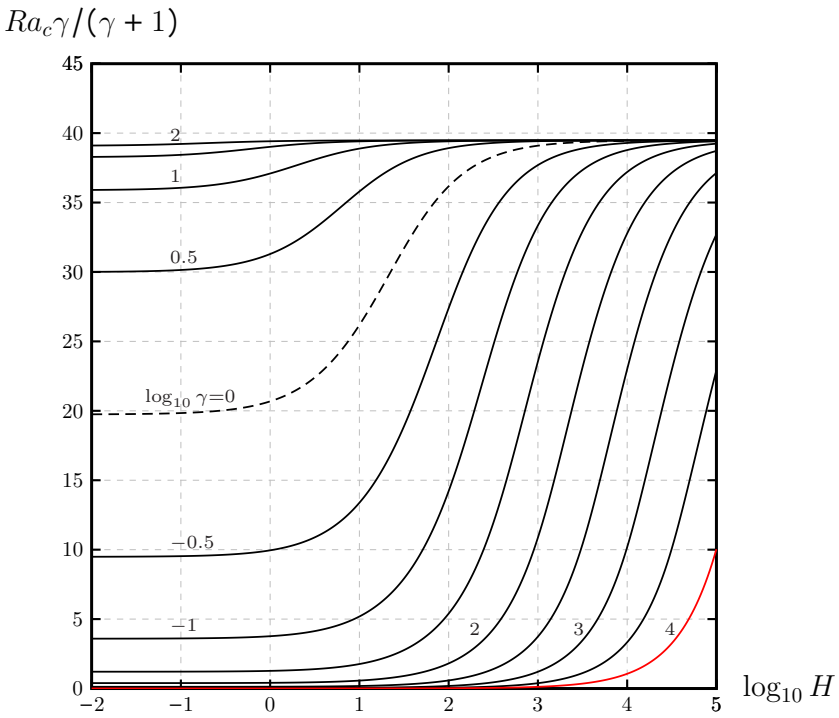

Figure 1: Showing the variation of the critical value of the porous-medium-based Darcy-Rayleigh number, $\mathrm{Ra}_0^* = \gamma \mathrm{Ra}/(\gamma+1)$, with $\log_{10} H$ for different values of $\log_{10}\gamma$. The red curve corresponds to $\gamma = 10^{-4}$ and the dashed line to $\gamma = 1$.

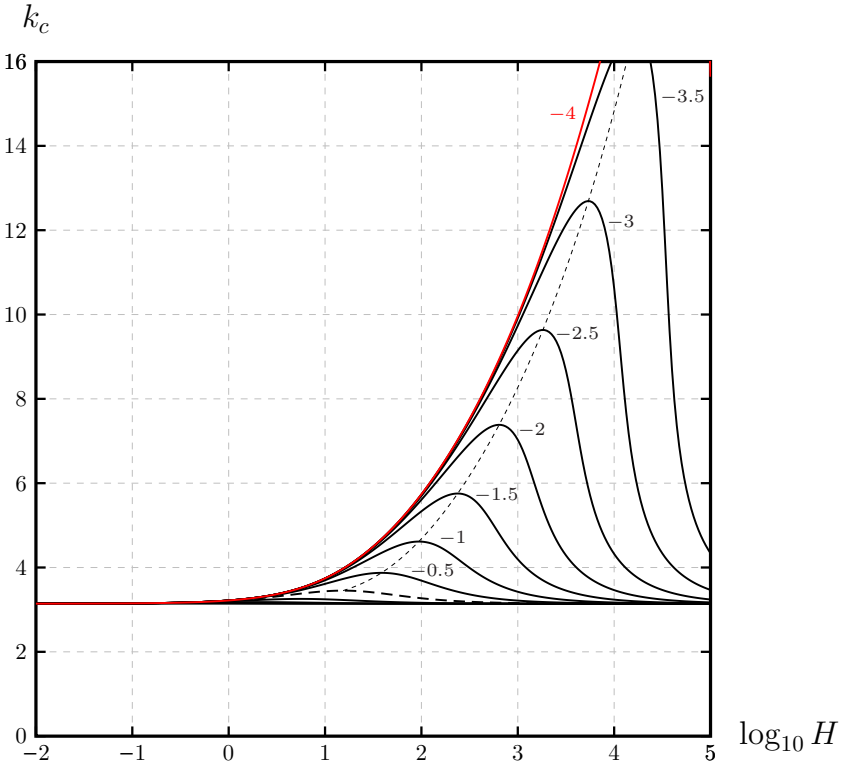

Figure 2: Showing the variation of the critical wavenumber, k, with $\log_{10} H$ for different values of $\log_{10} \gamma$. The red line corresponds to $\gamma = 10^{-4}$. The dashed line corresponds to $\gamma = 1$ and the dotted line to the locus of the largest critical wavenumber for each value of γ.

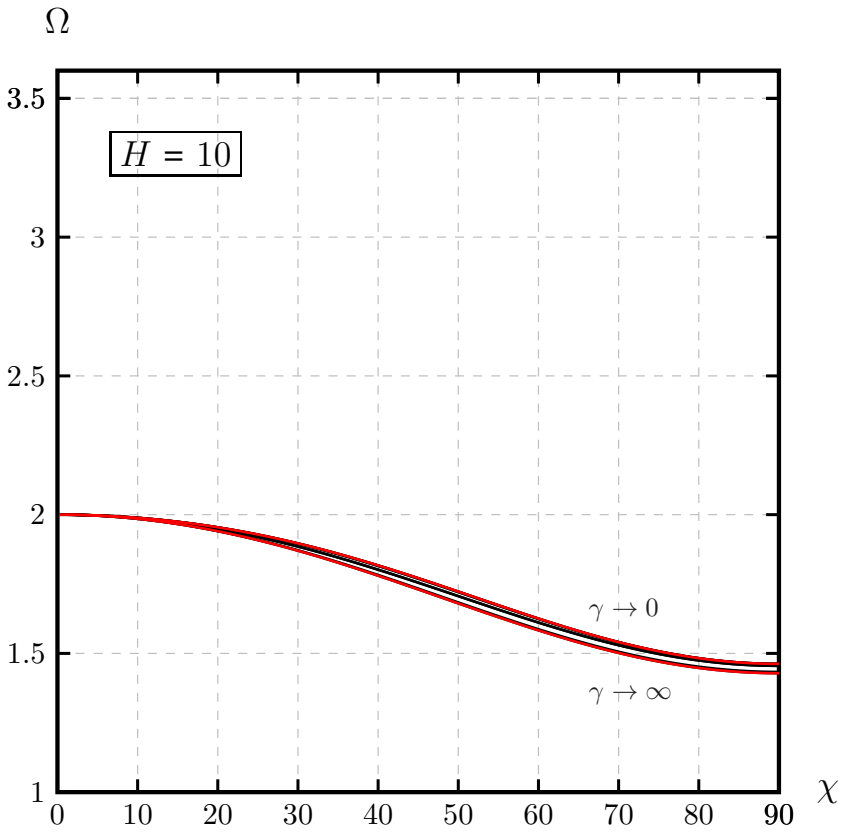

Figure 3: Displaying the variation with χ of the coupling coefficient, Ω, for $H = 10$ and for some selected values of $\log_{10}\gamma$. The clearest black line corresponds to $\log_{10}\gamma = 0$. The red lines correspond to $\gamma \to 0$ (upper) and $\gamma \to \infty$ (lower).

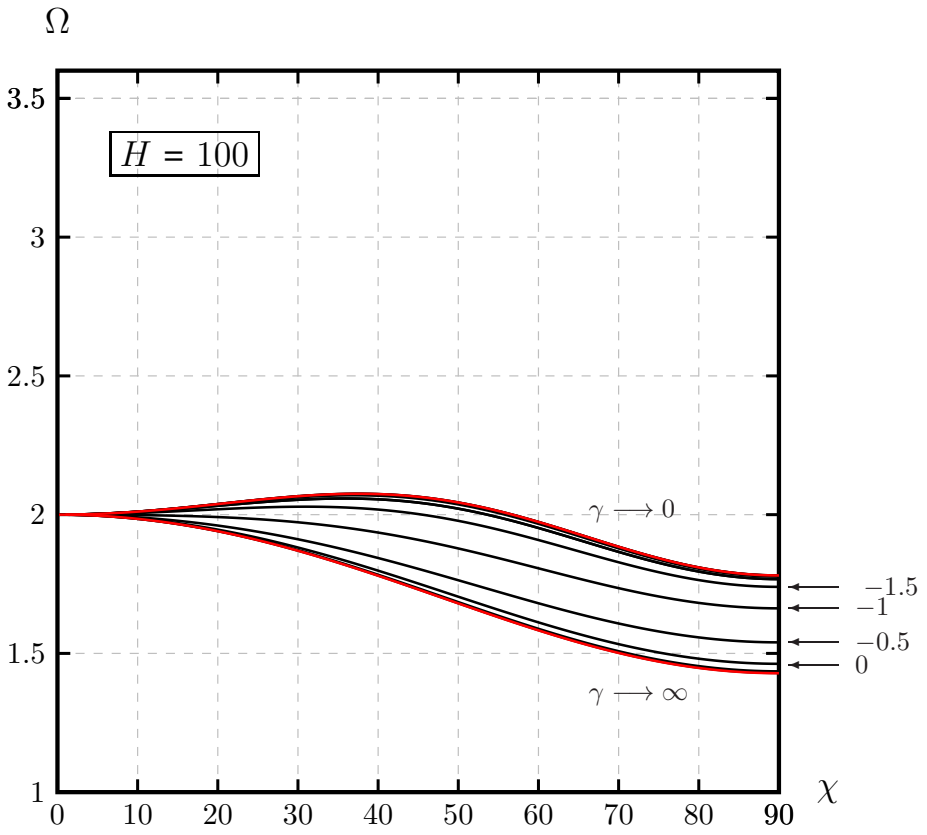

Figure 4: Displaying the variation with χ of the coupling coefficient, Ω, for $H = 100$ and for selected values of $\log_{10}\gamma$. The red lines correspond to $\gamma \to 0$ (upper) and $\gamma \to \infty$ (lower). The annotated numbers represent the values of $\log_{10}\gamma$.

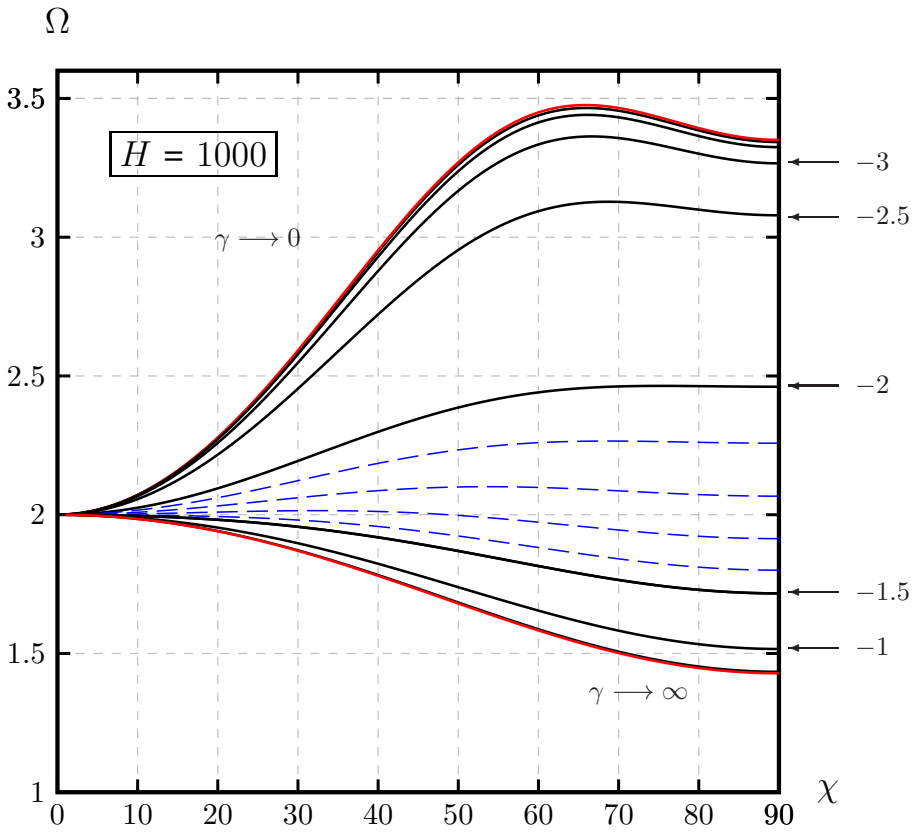

Figure 5: Displaying the variation with χ of the coupling coefficient, Ω, for $H = 1000$ and for selected values of $\log_{10}\gamma$. The red lines correspond to $\gamma \to 0$ (upper) and $\gamma \to \infty$ (lower). The annotated numbers represent the values of $\log_{10}\gamma$. The blue curves represent equally-spaced values of $\log_{10}\gamma$ between the neighbouring black lines.

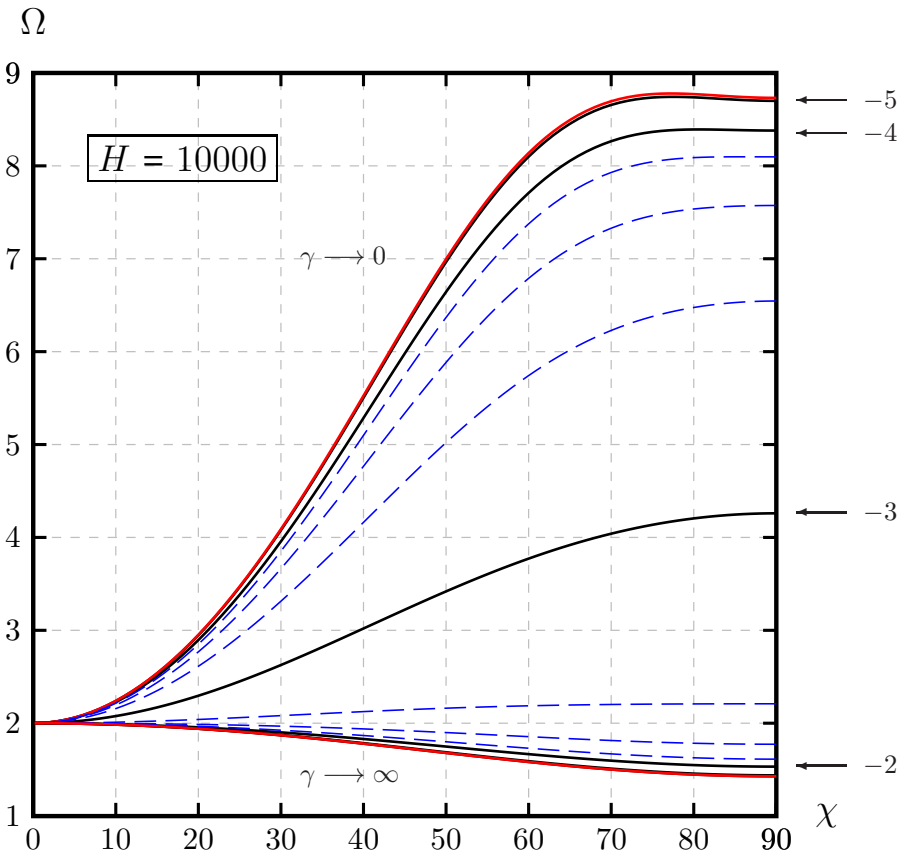

Figure 6: Displaying the variation with χ of the coupling coefficient, Ω, for $H = 10000$ and for selected values of $\log_{10}\gamma$. The red lines correspond to $\gamma \to 0$ (upper) and $\gamma \to \infty$ (lower). The annotated numbers represent the values of $\log_{10}\gamma$. The blue curves represent equally-spaced values of $\log_{10}\gamma$ between the neighbouring black lines.

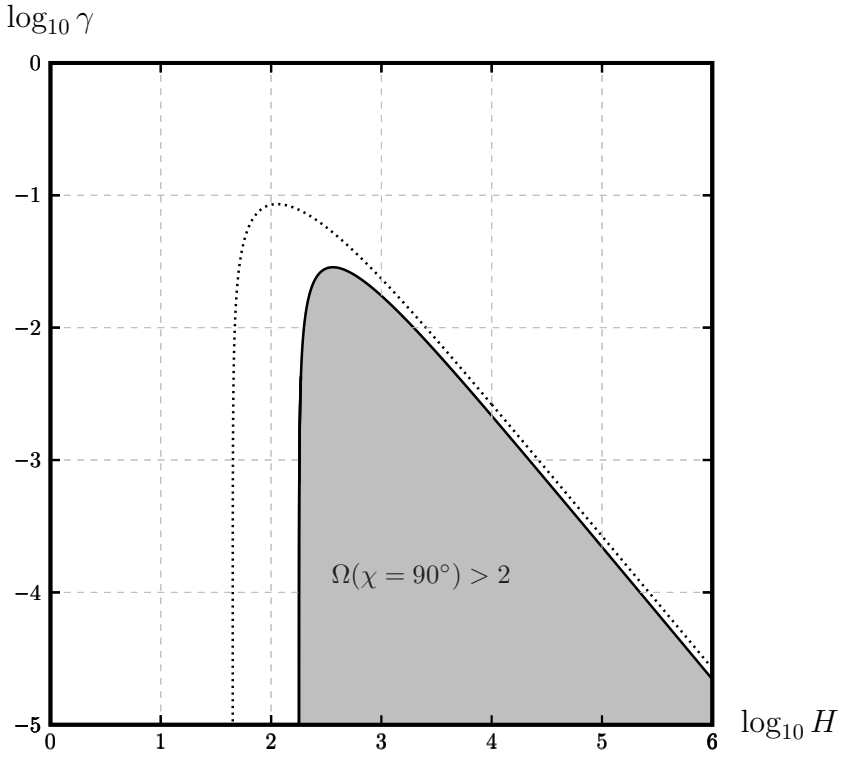

Figure 7: Depicting the region in (H, γ)-space where $\Omega(\chi = 90^\circ) > 2$ (grey shading). The white region corresponds to $\Omega(\chi = 90^\circ) < 2$ within which the cross-roll instability may be active. The dotted line corresponds to where $d^2\Omega/d\chi^2 = 0$ at $\chi = 0$.

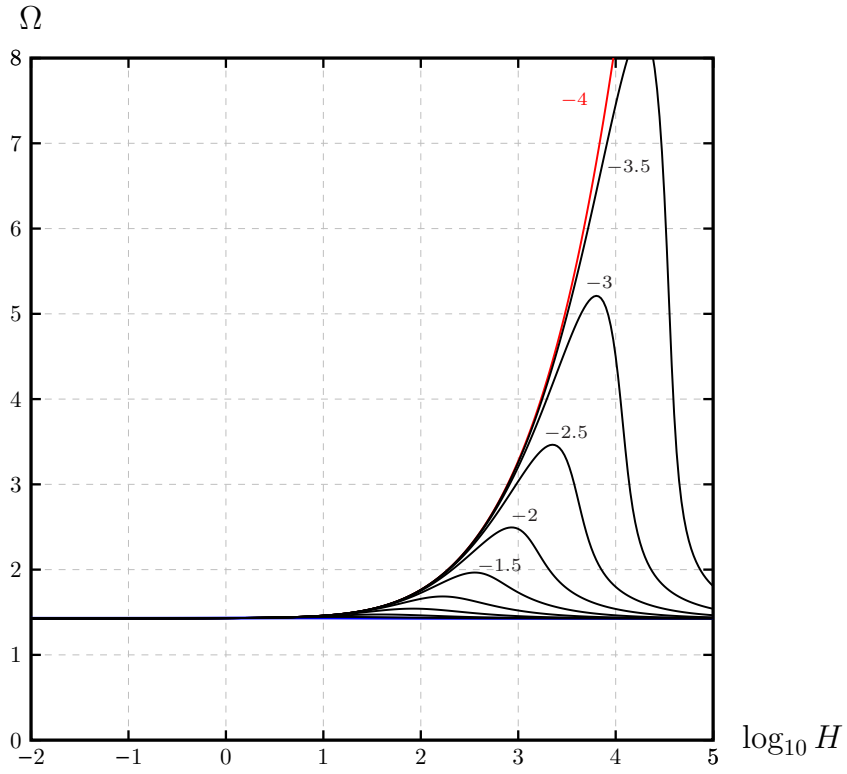

Figure 8: Showing the variation of the coupling/interaction constant, Ω, with $\log_{10} H$ for different values of γ. The red line corresponds to $\log_{10} \gamma = -4$ and this line is indistinguishable from the limit as $\gamma \to 0$. Other values of $\log_{10} \gamma$ are as indicated.